






Comparative Efficacy of Mayaro Virus-Like Particle Vaccines Produced in Insect or Mammalian Cells

 Sandra R. Abbo,^a Wilson Nguyen,^b Marleen H. C. Abma-Henkens,^a Denise van de Kamer,^a Niek H. A. Savelkoul,^a Corinne Geertsema,^a Thuy T. T. Le,^b Bing Tang,^b Kexin Yan,^b Troy Dumenil,^b Monique M. van Oers,^a  Andreas Suhrbier,^{b,c}  Gorben P. Pijlman^a

^aLaboratory of Virology, Wageningen University & Research, Wageningen, the Netherlands

^bInflammation Biology Group, QIMR Berghofer Medical Research Institute, Brisbane, Queensland, Australia

^cGVN Center of Excellence, Australian Infectious Disease Research Center, Brisbane, Queensland, Australia

Sandra R. Abbo and Wilson Nguyen contributed equally to this work. Author order is based on research contributions.

ABSTRACT Mayaro virus (MAYV) is a mosquito-transmitted alphavirus that causes often debilitating rheumatic disease in tropical Central and South America. There are currently no licensed vaccines or antiviral drugs available for MAYV disease. Here, we generated Mayaro virus-like particles (VLPs) using the scalable baculovirus-insect cell expression system. High-level secretion of MAYV VLPs in the culture fluid of Sf9 insect cells was achieved, and particles with a diameter of 64 to 70 nm were obtained after purification. We characterize a C57BL/6J adult wild-type mouse model of MAYV infection and disease and used this model to compare the immunogenicity of VLPs from insect cells with that of VLPs produced in mammalian cells. Mice received two intramuscular immunizations with 1 μ g of nonadjuvanted MAYV VLPs. Potent neutralizing antibody responses were generated against the vaccine strain, BeH407, with comparable activity seen against a contemporary 2018 isolate from Brazil (BR-18), whereas neutralizing activity against chikungunya virus was marginal. Sequencing of BR-18 illustrated that this virus segregates with genotype D isolates, whereas MAYV BeH407 belongs to genotype L. The mammalian cell-derived VLPs induced higher mean neutralizing antibody titers than those produced in insect cells. Both VLP vaccines completely protected adult wild-type mice against viremia, myositis, tendonitis, and joint inflammation after MAYV challenge.

IMPORTANCE Mayaro virus (MAYV) is associated with acute rheumatic disease that can be debilitating and can evolve into months of chronic arthralgia. MAYV is believed to have the potential to emerge as a tropical public health threat, especially if it develops the ability to be efficiently transmitted by urban mosquito vectors, such as *Aedes aegypti* and/or *Aedes albopictus*. Here, we describe a scalable virus-like particle vaccine against MAYV that induced neutralizing antibodies against a historical and a contemporary isolate of MAYV and protected mice against infection and disease, providing a potential new intervention for MAYV epidemic preparedness.

KEYWORDS Mayaro virus, vaccine, mouse model, virus-like particle, baculovirus

The tropical regions of our planet harbor a large diversity of mosquito-borne viruses, some of which have shown the potential to spread rapidly across human populations and cause large disease outbreaks. The latest wave of chikungunya virus (CHIKV) epidemics began in 2004 in East Africa, and in subsequent years CHIKV spread across the globe, resulting in >10 million cases in >100 countries on four continents (1, 2). Zika virus (ZIKV) spread from Africa via Asia and the Pacific Islands to Latin America, where, in 2015 and 2016, it was associated with a series of congenital, primarily neurological, malformations collectively known as congenital Zika syndrome (3, 4). These

Editor Mark T. Heise, University of North Carolina at Chapel Hill

Copyright © 2023 American Society for Microbiology. All Rights Reserved.

Address correspondence to Andreas Suhrbier, Andreas.Suhrbier@qimrberghofer.edu.au, or Gorben P. Pijlman, gorben.pijlman@wur.nl.

The authors declare no conflict of interest.

Received 15 October 2022

Accepted 13 February 2023

Published 8 March 2023

two viruses moved from a primarily sylvatic environment and entered into urban transmission cycles involving humans and anthropophilic mosquito species, such as the yellow fever mosquito *Aedes aegypti*. Mayaro virus (MAYV) may also have this potential and thereby could emerge as a more important threat to public health (5). In tropical rainforests, MAYV is maintained in an enzootic transmission cycle between nonhuman primates and forest-dwelling *Haemagogus* mosquito species (6, 7). A key step toward urban spread would be acquisition by MAYV of the ability to be efficiently transmitted by urban vectors, such as the aforementioned *Aedes* species (8–11). Laboratory transmission studies using these mosquitoes suggest that, although MAYV can replicate, at realistic blood meal titers dissemination into the salivary glands is limited (10, 12–14).

MAYV is associated with an increasing number of reports of human infections in Central and South America (6, 15, 16), with imported cases in several European countries (8, 17) and the United States (18). In 2015, a child with no travel history from rural or semirural areas of Haiti was diagnosed with a coinfection of MAYV and dengue virus, suggesting transmission outside tropical rainforest settings (19). MAYV is a member of the arthritogenic group of alphaviruses that show broadly similar patterns of rheumatic disease in humans (20, 21) and also collectively belong to the Semliki Forest antigenic complex (22). Symptomatic MAYV infection in humans is associated with acute rheumatic disease comprising primarily fever, myalgia, rash, and polyarthralgia, with the latter persisting for months in some patients (6, 15, 20). Rare severe forms of MAYV disease can include encephalitis or meningoencephalitis and hemorrhagic manifestations, although fatality is extremely rare (15, 23).

Like all alphaviruses, MAYV has an ~11.5-kb, single-stranded, positive-sense RNA genome that encodes four nonstructural proteins (nsP1 to nsP4) in a single open reading frame (ORF), and immediately downstream is a second ORF coding for the structural proteins. The structural proteins include the capsid protein or C and the two envelope glycoproteins E2 and E1, with their associated proteins E3 and 6K, respectively, and the transframe protein TF (resulting from a –1 ribosomal frameshift in 6K) (24, 25). The nonstructural proteins are involved in replication of the RNA genome, whereas the structural proteins form a spherical virus particle of ~70 nm in diameter with a T = 4 icosahedral symmetry (24). C binds the viral RNA and forms the internal core of ~40 nm in diameter (24), which is enveloped by a host-derived lipid bilayer containing the envelope glycoproteins (26). The 240 E2-E1 heterodimers found on the surface of the virion form 80 trimeric spikes (26), which have important functions in virus assembly, receptor recognition, and entry into cells (27) and are the antigens of choice for vaccine development (22, 28–32).

There are currently no licensed vaccines or antiviral drugs for MAYV (23), although alphaviral arthritides are widely treated with nonsteroidal anti-inflammatory drugs (20, 21). Several effective preclinical MAYV vaccines have been developed, including a live-attenuated vaccine (28, 29), a DNA vaccine (30), and two adenoviral-vectored vaccines (31, 32). Induction of arthralgia by TSI-GSD-218, a live-attenuated CHIKV vaccine (33), has slowed the development of live-attenuated vaccines for arthritogenic alphaviruses; however, a rationally attenuated CHIKV vaccine has demonstrated an acceptable safety profile and has entered late-phase clinical trials. DNA vaccines are an attractive candidate due to their efficient production process and long shelf-life, but they often show poor immunogenicity in humans (34). Efficacy of adenoviral-vectored vaccines can be compromised by the existence and/or development of antivector immunity (35).

Here, we report the development of an enveloped MAYV virus-like particle (VLP) from insect cells. Self-assembly of the envelope and capsid proteins results in formation of enveloped VLPs, which are structurally similar to the virus particle but do not contain a viral genome and are thus unable to cause a spreading infection (36–38). The size of VLPs (20 to 200 nm) is optimal for uptake by antigen-presenting cells and cross-presentation (39). The highly repetitive surface structures on the VLPs also lead to the activation of innate immunity and ultimately increased antibody production, often without the need for adjuvants (40). Here, we compare insect cell-derived MAYV VLPs

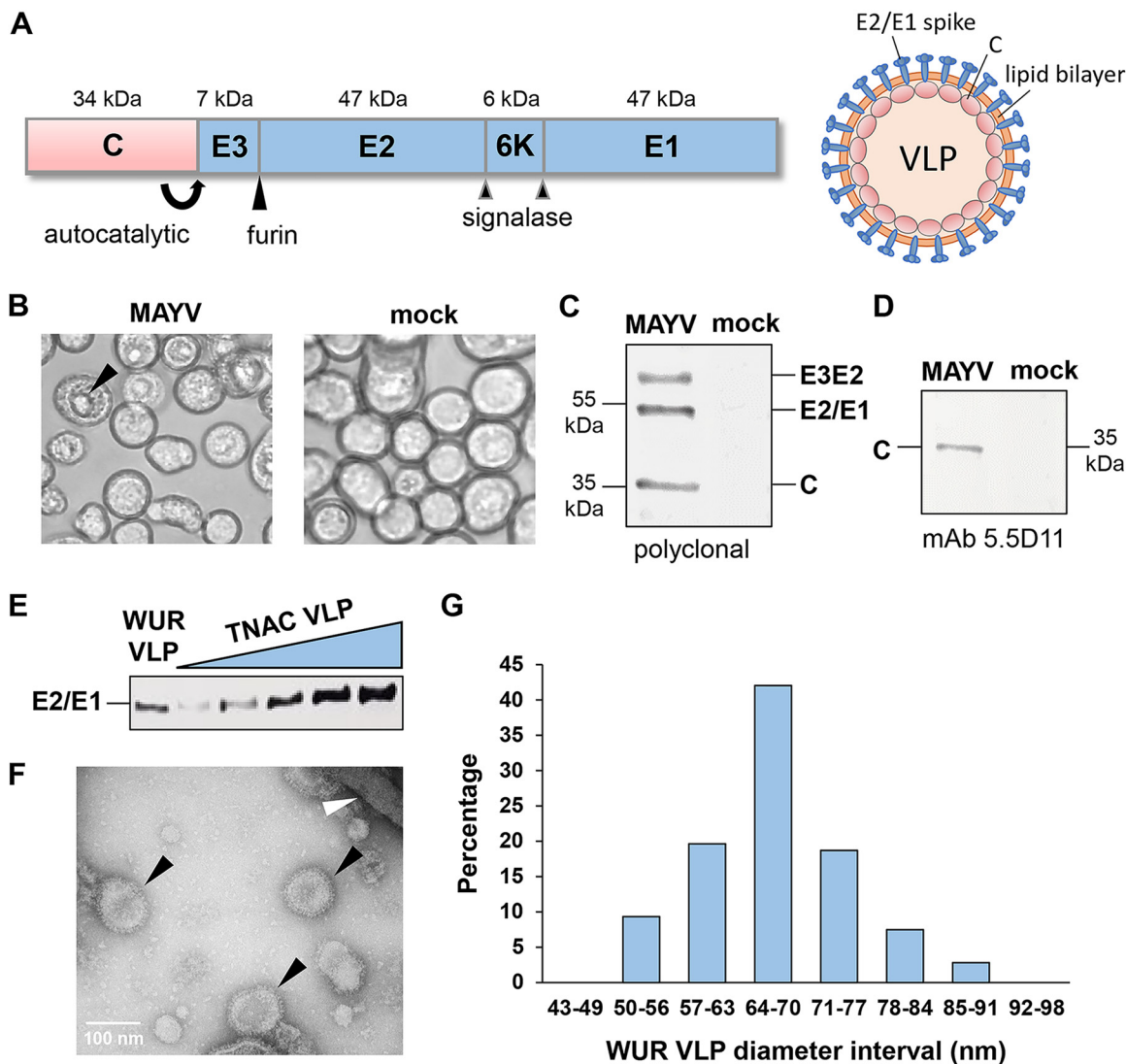


FIG 1 MAYV VLP production using insect cells and recombinant baculoviruses. (A) Schematic overview of the MAYV structural cassette expressed in insect cells. The molecular weight of each protein is shown in kilodaltons. Autocatalytic, host furin, and host signalase cleavage sites are indicated. (B) BACe56/MAYV-infected Sf9 insect cells and mock-infected Sf9 insect cells at 4 days postinfection. Black arrow indicates dense nuclear body, which presumably consisted of accumulated MAYV core-like particles. (C and D) MAYV structural protein expression in Sf9 cells was analyzed at 4 days postinfection by western blotting using antiserum derived from a MAYV-infected mouse (C) or anti-CHIKV capsid antibody 5.5D11 (D). (E) Detection of MAYV structural proteins in purified WUR VLP fraction from Sf9 insect cells and dilution series of TNAC MAYV VLPs from HEK293 human cells. (F) Transmission electron microscopy photo of purified WUR MAYV VLPs. Black arrows indicate MAYV VLPs; white arrow indicates baculovirus. (G) Size distribution of WUR MAYV VLPs based on diameter measurements of 107 VLPs.

with those expressed in mammalian cell culture and evaluate these vaccine candidates in an adult wild-type mouse model of MAYV infection and disease.

RESULTS

Production of MAYV VLPs in insect cells. To produce MAYV VLPs in Sf9 insect cells, a recombinant baculovirus, BACe56/MAYV, expressing the structural cassette of MAYV (Fig. 1A) was generated. At 4 days postinfection, accumulation of alphavirus capsid proteins was observed in the nuclei (Fig. 1B, arrowhead), as seen previously for CHIKV and salmonid alphavirus structural protein expression (41, 42). MAYV protein expression was confirmed by western blotting. Detection with mouse polyclonal antiserum (from a MAYV-infected mouse) resulted in two bands of ~55 kDa (Fig. 1C), corresponding to the predicted molecular weights of precursor E3-E2 (54 kDa) and E2

and/or E1 (47 kDa each), and one band corresponding to the predicted molecular weight of capsid (34 kDa) (Fig. 1C). The presence of MAYV capsid was confirmed with monoclonal antibody 5.5D11, which recognizes capsid from multiple alphaviruses in the Semliki Forest serogroup (43) (Fig. 1D).

For large-scale MAYV VLP production, Sf9 suspension cells were infected with recombinant baculovirus at a low multiplicity of infection (MOI). At 4 days postinfection, the VLPs in the culture fluid were precipitated with polyethylene glycol (PEG) and purified on a sucrose gradient. VLPs were quantified by western blot analysis using a dilution series of commercially available VLPs from The Native Antigen Company (TNAC), which were produced in the human HEK293 cell line (Fig. 1E). VLPs were analyzed by transmission electron microscopy, and enveloped spherical particles were observed (Fig. 1F, black arrowheads). Some baculovirus particles could also be seen (Fig. 1F, white arrowhead); complete removal of baculoviruses from the final vaccine preparation presented a challenge, as physical properties, structures, and sizes of the VLPs and the baculovirus virions are similar (38, 44). MAYV VLPs were between 64 and 70 nm in diameter (Fig. 1G), which conformed to the reported size of alphavirus virions (24, 45).

MAYV BeH407 replication and pathogenesis in C57BL/6J adult mice. To evaluate the MAYV VLPs for use in vaccine development, an adult wild-type mouse model of MAYV infection and disease was first established and characterized, based on previously described adult mouse models (29, 46). Adult 6- to 24-week-old female C57BL/6J mice were infected subcutaneously in the hind feet with MAYV BeH407 at doses of 10^4 , 10^5 , or 10^6 50% tissue culture infectious doses (TCID₅₀). Viremia for mice infected with 10^4 TCID₅₀ and 10^5 TCID₅₀ peaked on day 2 postinfection, compared to that in mice infected with 10^6 TCID₅₀, which peaked on day 1 postinfection (Fig. 2A). Peak foot swelling, an indicator of arthritic disease, was observed on day 6 postinfection for all doses (Fig. 2B), with a dose of 10^5 TCID₅₀ resulting in an increase in foot swelling of $\approx 20\%$. Hematoxylin and eosin (H&E) staining of these arthritic feet illustrated the characteristic mononuclear cellular infiltrates (20, 22, 47), which were evident in muscle tissue (black ovals), tendons, synovial spaces, and in regions of subcutaneous edema (Fig. 2C). Quantitation using purple (nuclear) versus red (cytoplasmic) staining ratios, a measure of leukocyte infiltration (48), demonstrated significant differences between MAYV-infected mice compared to mock-infected mice (Fig. 2D). Thus, infection of C57BL/6J mice with the human isolate, MAYV BeH407, provided an adult wild-type MAYV mouse model that recapitulated viremia and histological features characteristic of alphaviral arthritides (20, 21).

Immunogenicity of MAYV VLP vaccines and neutralizing antibody responses against MAYV isolates and CHIKV. To determine whether MAYV VLPs could induce a protective immune response against MAYV infection, groups of adult 6- to 8-week-old female C57BL/6J mice were immunized with one or two doses of 1 μ g insect cell-derived "Wageningen University & Research" (WUR) VLPs (with or without adjuvant) (49), and antibody responses and protection against disease were determined (Fig. 3A). For comparison, another group of mice was vaccinated with 1 μ g of HEK293 cell-derived "The Native Antigen Company" (TNAC) VLPs without adjuvant. As a negative control, mice were mock vaccinated with RPMI 1640 medium. After one vaccination, MAYV-specific antibodies were observed by enzyme-linked immunosorbent assay (ELISA) for both WUR VLPs and TNAC VLPs. TNAC VLPs induced significantly higher ELISA responses than WUR VLPs (Fig. 3B) and also higher levels of neutralizing antibodies (Fig. 3C). No significant effect of the adjuvant on the immunogenicity of WUR VLPs was observed (Fig. 3B and C). Next, mice were boosted with 1 μ g of the respective VLPs, except for the group WUR VLP with adjuvant. Vaccination with $2 \times 1 \mu$ g of WUR VLP or TNAC VLP generated high ELISA responses (Fig. 3B) and neutralizing antibody responses (Fig. 3C). Again, TNAC VLPs induced significantly higher ELISA and mean neutralization titers than WUR VLPs (Fig. 3B and C). Vaccination with one dose of 1 μ g of WUR VLP with adjuvant also generated ELISA and neutralizing responses after 8 weeks, but these were significantly lower than responses in the group with two doses of nonadjuvanted WUR VLPs at 8 weeks (Fig. 3B and C).

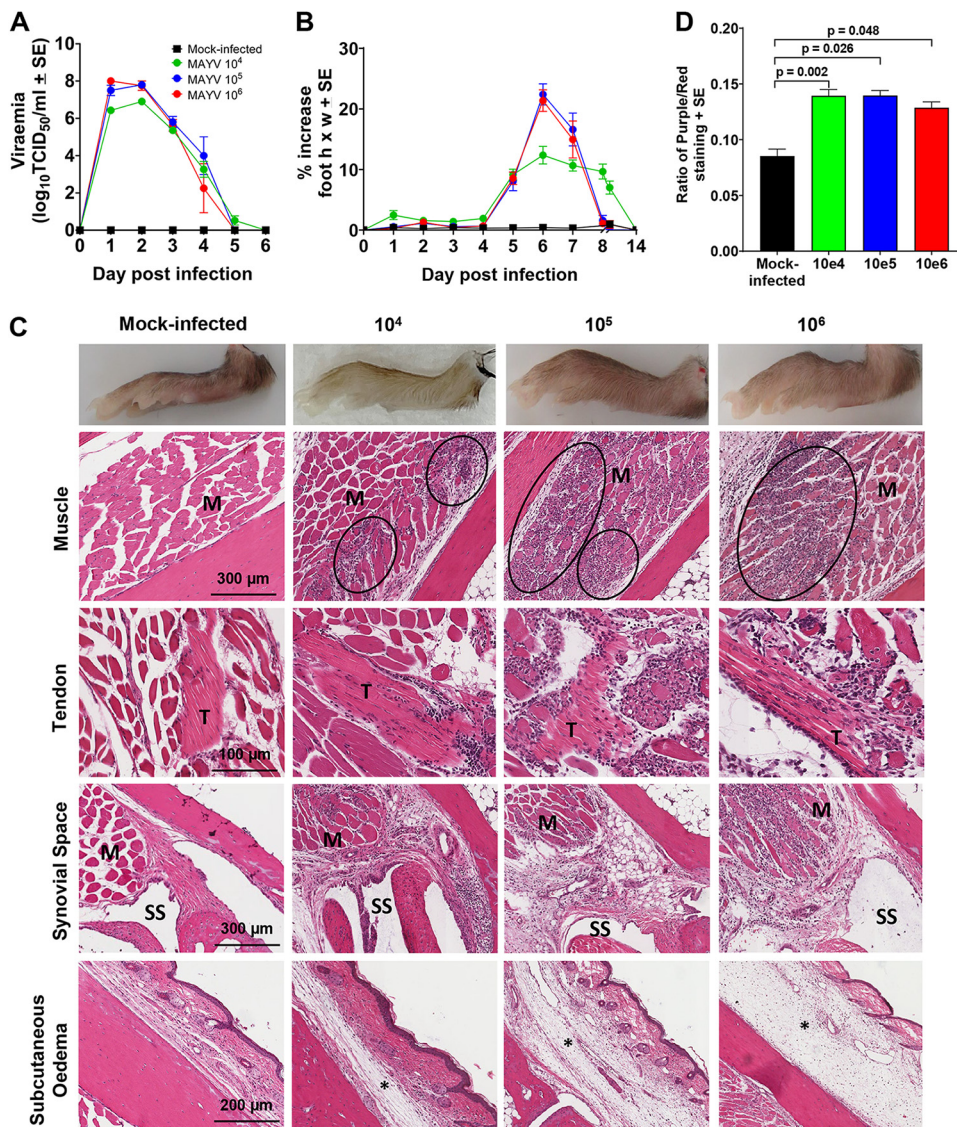


FIG 2 MAYV BeH407 in adult wild-type C57BL/6J mice. (A) Viremia in adult female C57BL/6J mice (6 to 24 weeks old) infected with 10^4 , 10^5 , or 10^6 TCID₅₀ or mock-infected with PBS, with $n = 4$ to 6 mice per group. (B) Percentage increase in foot height \times width (relative to day 0) for mice infected as described for panel A, with $n = 8$ to 12 feet from 4 to 6 mice per group per time point. (C) Photographs showing examples of feet on day 6 postinfection, illustrating foot swelling in MAYV-infected groups compared to the mock-infected control group. H&E staining of muscle (M), tendon (T), synovial space (SS), and subcutaneous edema (*) in foot sections from 6- to 24-week-old C57BL/6J wild-type female mice infected as described for panel A. Black ovals indicate some of the areas containing inflammatory infiltrates in the muscles. Inflammatory infiltrates near and in tendon areas are visible, as well as inflammatory infiltrates near joint tissues. (D) Ratio of nuclear (purple) to nonnuclear (red) staining of H&E-stained foot sections (a measure of leukocyte infiltration). Data from 4 to 6 feet from 2 to 3 mice per group, with 3 sections scanned per foot and values averaged to produce one value for each foot. Statistical analysis used the Kolmogorov-Smirnov test. Multiple test correction was not applied. Error bars indicate one standard error of the mean.

Neutralization titers were also determined for a contemporary MAYV isolate, the BR-18 strain (50), as well as for CHIKV (Reunion Island isolate). Neutralizing antibody titers against MAYV BeH407 (Fig. 3D) were comparable to those seen for MAYV BR-18 (Fig. 3E). However, these sera showed poor or no detectable neutralizing activity against CHIKV (Fig. 3F).

Evaluation of VLP vaccines against MAYV infection and disease in C57BL/6J mice. To evaluate protection against disease, mice were challenged with MAYV BeH407 6 weeks after the second vaccination. A challenge dose of 10^5 TCID₅₀ was used, as this dose induced $\approx 20\%$ foot swelling, with the lower dose inducing less foot swelling and no increase in foot swelling seen with the higher dose (Fig. 2B). Two doses of $1 \mu\text{g}$ of

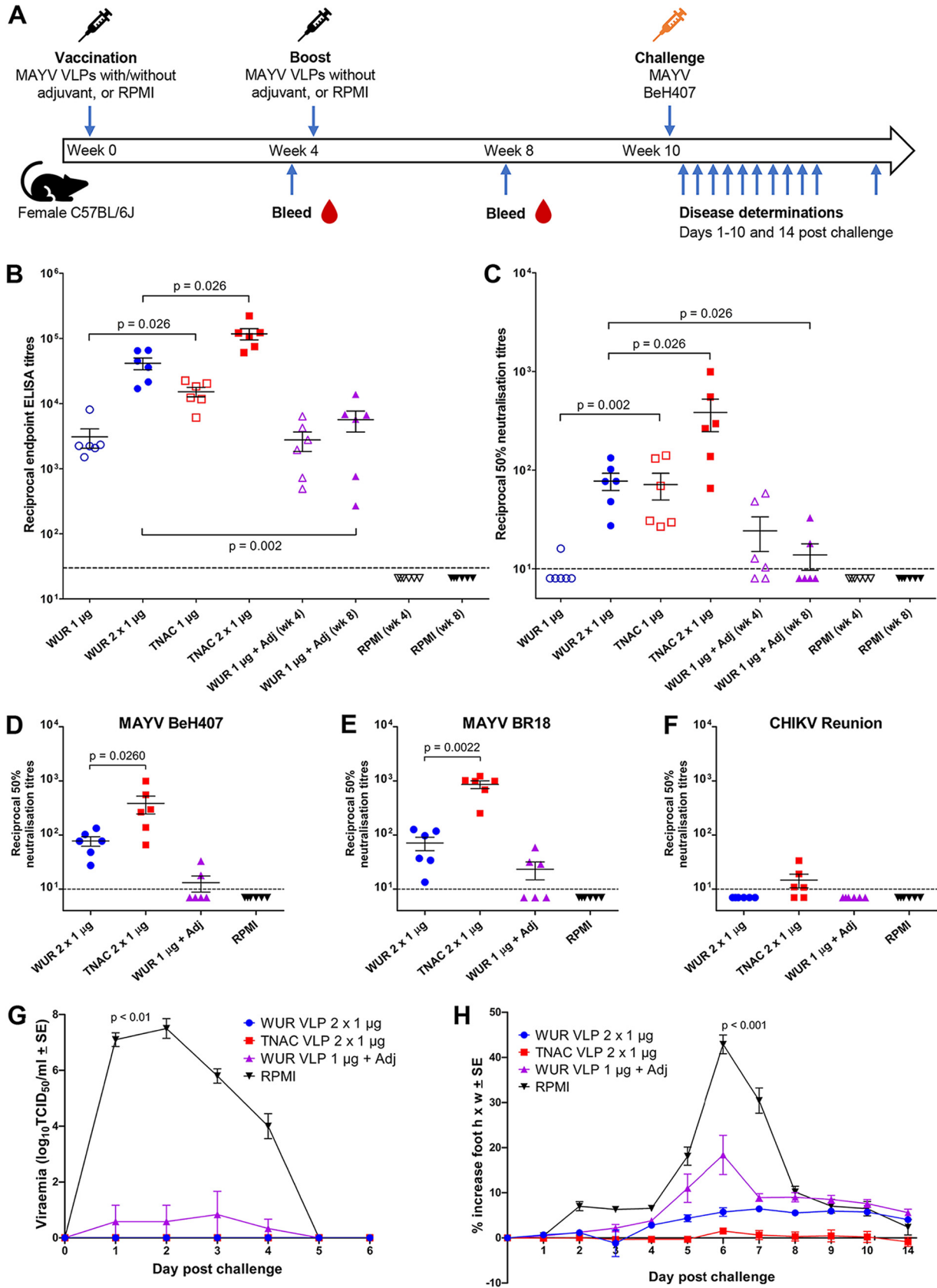


FIG 3 MAYV VLP vaccination and challenge with MAYV BeH407 in adult C57BL/6J mice. (A) Timeline of vaccination with two 1-µg doses of nonadjuvanted MAYV VLPs, with a single 1-µg dose of adjuvanted MAYV VLPs, or with two doses of RPMI 1640 medium (negative control), (Continued on next page)

WUR VLP or TNAC VLP provided statistically significant protection against viremia, with no virus detected in the sera of any vaccinated mice ($P < 0.01$ for days 1 to 4 postchallenge) (Fig. 3G). One dose of 1 μg of WUR VLP with adjuvant also showed a significant reduction in viremia, although complete protection in all mice was not observed (Fig. 3G). In addition, two doses of 1 μg of WUR VLP or TNAC VLP were sufficient to provide protection against MAYV-induced foot swelling (both $P < 0.001$ compared to mock-vaccinated) (Fig. 3H), while one dose of 1 μg of WUR VLP with adjuvant demonstrated only partial protection against foot swelling. Thus, two doses of 1 μg nonadjuvanted MAYV VLPs generated ELISA responses and neutralization antibodies sufficient for complete protection against viremia and arthritic disease. Future studies could focus on selecting adjuvants allowing single-shot administration with a long duration of immunity.

Histopathology of vaccinated C57BL/6J mice after MAYV challenge. H&E staining of feet from mice at 6 days postchallenge illustrated the characteristic mononuclear cellular infiltrates (22, 47, 51) evident in muscle tissues (black ovals), in tendons, in surrounding joint areas, and in regions of subcutaneous edema in the mock-vaccinated RPMI control group and in the group that had received one shot of WUR VLP with adjuvant (Fig. 4A; full-size images are provided in Fig. S1 in the supplemental material). Hemorrhage was also observed in the mock-vaccinated RPMI control group (Fig. 4A, arrows). Mice vaccinated with two shots of VLPs (either WUR or TNAC) showed healthy tissues without cellular infiltrates. Quantitation using purple (nuclear) versus red (cytoplasmic) staining ratios (Fig. 4B) demonstrated no statistically significant differences between mice that had received two doses of the WUR VLP compared to those that received two doses of the TNAC VLP. Significant differences were observed between mice which had received two doses of the WUR VLP or two doses of the TNAC VLP compared to the mock RPMI-vaccinated, infected mice. Two doses of the WUR VLP or TNAC VLP thus provided protection against myositis, tendonitis, arthritis and hemorrhage.

Sequencing of MAYV BR-18. We undertook full-genome sequencing for MAYV BR-18, a 2018 isolate from Brazil (50), that was used here in neutralization assays (Fig. 3E). This isolate showed no changes in the receptor (MXRA8) binding residues (52) compared with the 1955 MAYV BeH407 isolate, with both MAYV isolates showing only a 60% amino acid identity with CHIKV at these positions (Fig. 5A). These sequence data were consistent with our neutralization data (Fig. 3D to F), as well as previous MAYV-CHIKV cross-neutralization studies (22). A series of amino acid changes in the structural proteins (that are not involved in receptor binding) were evident, but more than half (58.5%) were conserved substitutions (53), with most of the nonconserved amino acid changes falling near the contact zone between E1 and E2 (Fig. 5B). The results suggested that changes in the sequence of MAYV over time are not accompanied by major changes in key determinants, and ensuing escape from vaccines based on earlier sequences.

Three genotypes have been described for MAYV: D (widely disperse), L (limited), and N (new) (54). A dendrogram of complete genome nucleotide sequences suggests that BR-18 segregates with genotype D viruses, although it sits alone and somewhat apart from other genotype D isolates (Fig. S2). BR-18 also segregates with genotype D viruses in a dendrogram of E2-E1 amino acid sequences, clustering with a much older

FIG 3 Legend (Continued)

then antibody measurements after bleeds, and disease determinations of viremia and foot swelling following MAYV BeH407 challenge. (B) MAYV BeH407 endpoint IgG ELISA titers after 1 or 2 vaccinations of female 6- to 8-week-old C57BL/6J mice with nonadjuvanted MAYV VLPs or RPMI control, or 1 vaccination with MAYV VLPs with adjuvant. Lines among the dots indicate the mean ELISA titers, and error bars show the standard errors of the means. Dashed line represents the limit of detection (1:30 serum dilution). Statistical analysis used the Kolmogorov-Smirnov test. Multiple test correction was not applied. (C) MAYV BeH407 50% neutralization titers after 1 or 2 vaccinations with nonadjuvanted MAYV VLPs or RPMI control, or 1 vaccination with MAYV VLPs with adjuvant. Lines among the dots indicate the mean neutralization titers, and error bars show the standard errors of the means. Dashed line represents the limit of detection (1:10 serum dilution). Statistical analysis was with the Kolmogorov-Smirnov test. Multiple test correction was not applied. (D to F) Comparison of neutralization titers at week 8 against MAYV BeH407 (D), MAYV BR-18 (E), and CHIKV (Reunion isolate) (F). (G) MAYV BeH407 viremia postchallenge in mice vaccinated twice with nonadjuvanted MAYV VLPs or RPMI, or vaccinated once with MAYV VLPs with adjuvant ($n = 5$ to 6 per group). The limit of detection for each mouse was 10^2 TCID₅₀/mL, with means from 5/6 mice plotted. Statistical analysis was with the Kolmogorov-Smirnov test. Multiple test correction was not applied. (H) Percentage increase in foot height \times width (relative to day 0) for C57BL/6J mice vaccinated as described for panel G, with $n = 6$ to 12 feet from 3 to 6 mice per group per time point. Statistical analysis was with the t test.

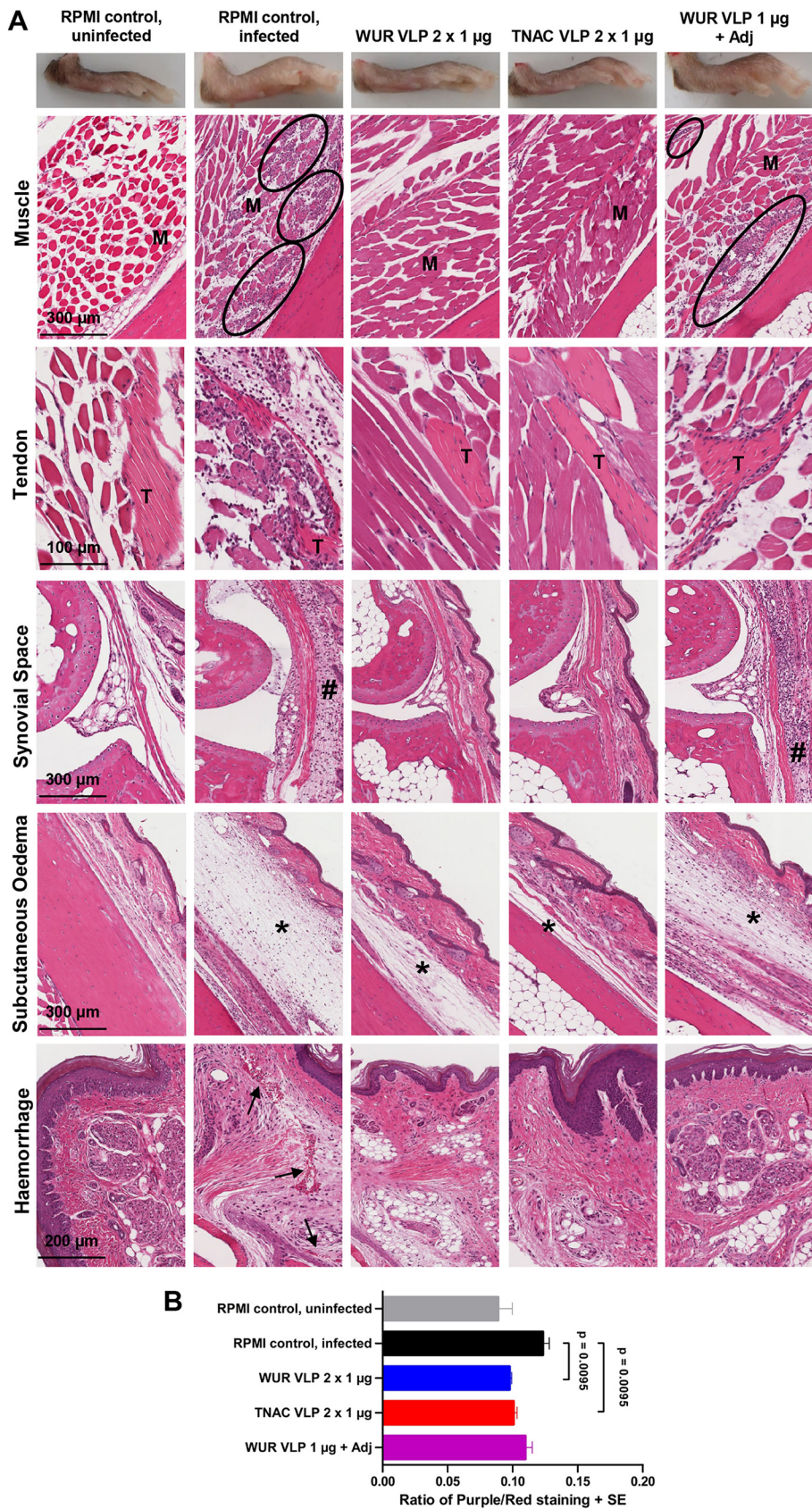


FIG 4 Histopathology of MAYV VLP-vaccinated adult C57BL/6J mice after challenge with MAYV BEH407. (A) Photographs of mouse feet at 6 days postchallenge, illustrating swelling on day 6 in the RPMI-vaccinated, (Continued on next page)

group of viruses isolated in the 1950s in Trinidad Tobago and the United States (Fig. S3). MAYV BeH407 clusters with genotype L (Fig. S2 and 3).

DISCUSSION

In this study, we developed a scalable MAYV VLP vaccine produced in insect cells which protected mice against viremia and arthritic disease in an adult wild-type mouse model of MAYV disease. Due to their phylogenetic proximity, with CHIKV and MAYV also belonging to the same serogroup (55, 56), it has been suggested that CHIKV vaccines (several are currently in human clinical trials [1, 57–59]) may confer some level of cross-protection against MAYV. However, a vaccinia-based CHIKV vaccine and an adenovirus vector-based CHIKV vaccine showed no or only partial cross-protection against MAYV (22, 31). Furthermore, a live-attenuated CHIKV vaccine and an insect-specific alphavirus-based CHIKV vaccine similarly failed to cross-protect against MAYV. Interestingly, wild-type CHIKV infection did confer cross-protection against MAYV, suggesting that high levels of natural CHIKV herd immunity in the neotropics may reduce the risk of MAYV emergence (56). In our study, sera from mice vaccinated with MAYV VLPs also showed no (or barely detectable) levels of cross-neutralization activity with CHIKV. We thus contend that reliance on a CHIKV vaccine in the event of a MAYV epidemic is not a viable strategy (22).

Two shots of 1 μ g WUR VLPs from insect cells were needed to induce high neutralizing antibody levels and to protect mice against MAYV disease. In contrast, high neutralizing antibody titers were already observed after a single vaccination with TNAC VLPs. Differences in protein glycosylation may explain these differences in immunogenicity (60–62). CHIKV VLPs from HEK293 cells contain oligomannose, hybrid, and complex glycans, whereas VLPs from insect cells mostly contain oligomannose glycans (63). Our recent glycosylation analysis of CHIKV spikes generated in Sf9 cells revealed that the majority of N-glycans were of the mannose or hybrid type, with <2% being complex glycans (64). Despite these notable differences in glycosylation, immunization of guinea pigs with CHIKV VLPs from either HEK293 or Sf cells yielded very similar neutralizing antibody responses (44), suggesting that the effect of different glycans may be dependent on vaccine dose and/or antigen. Conceivably, glycans may be more important for correct antigen folding and stability (62) of MAYV VLPs than for CHIKV VLPs. A structural comparison of WUR with TNAC VLPs, e.g., by cryo-electron microscopy, would be interesting to tease out potential differences in protein folding, but this would be best approached in a follow-up study. Another difference is that the VLPs from insect cells contain some residual baculovirus. For use in humans, VLP vaccines need to be highly purified and should not contain these contaminants. This can be accomplished by optimizing the VLP purification process or development of a baculovirus-based production system free of contaminating progeny baculovirus particles (38, 65).

In the MAYV mouse model described here, 10^5 TCID₅₀ of MAYV BeH407 induced mean arthritic foot swelling of $\approx 20\%$, whereas for 10^4 TCID₅₀ this dropped to $\approx 12\%$. In contrast, 10^4 TCID₅₀ CHIKV (Reunion isolate) in the same C57BL/6J mouse strain induced foot swelling of $>60\%$ (66, 67), although foot swelling was less pronounced for Asian and Caribbean isolates of CHIKV (68, 69). Different isolates of the same alphavirus can thus induce different levels of arthritic disease in these mouse models (22, 46). However, the MAYV mouse model may be recapitulating human disease, where MAYV is generally less severe (very few cases of mortality [23]) than CHIKV ($\approx 0.1\%$ mortality [1]), but it should be kept in mind that there may be differences in diagnosis and obtaining of epidemiological data.

FIG 4 Legend (Continued)

infected, and WUR VLP with adjuvant groups. H&E staining of tissues in foot sections from RPMI-vaccinated or VLP-vaccinated, uninfected, and MAYV-infected adult C57BL/6J mice is shown. Black ovals indicate some of the areas containing inflammatory infiltrates in the muscles (M). Inflammatory infiltrates near tendons (T) as well as inflammatory infiltrates near joint tissues (#) were also seen. Subcutaneous edema is shown with an asterisk. Hemorrhage is indicated by black arrows. These images are representative of a larger number analyzed. (B) Ratio of nuclear (purple) to nonnuclear (red) staining of H&E-stained foot sections ($n = 2$ to 3 mice, 4 to 6 feet per group, 3 sections per foot; values were averaged to produce one value for each foot). Statistical analysis used the Kolmogorov-Smirnov test. Multiple test correction was not applied.

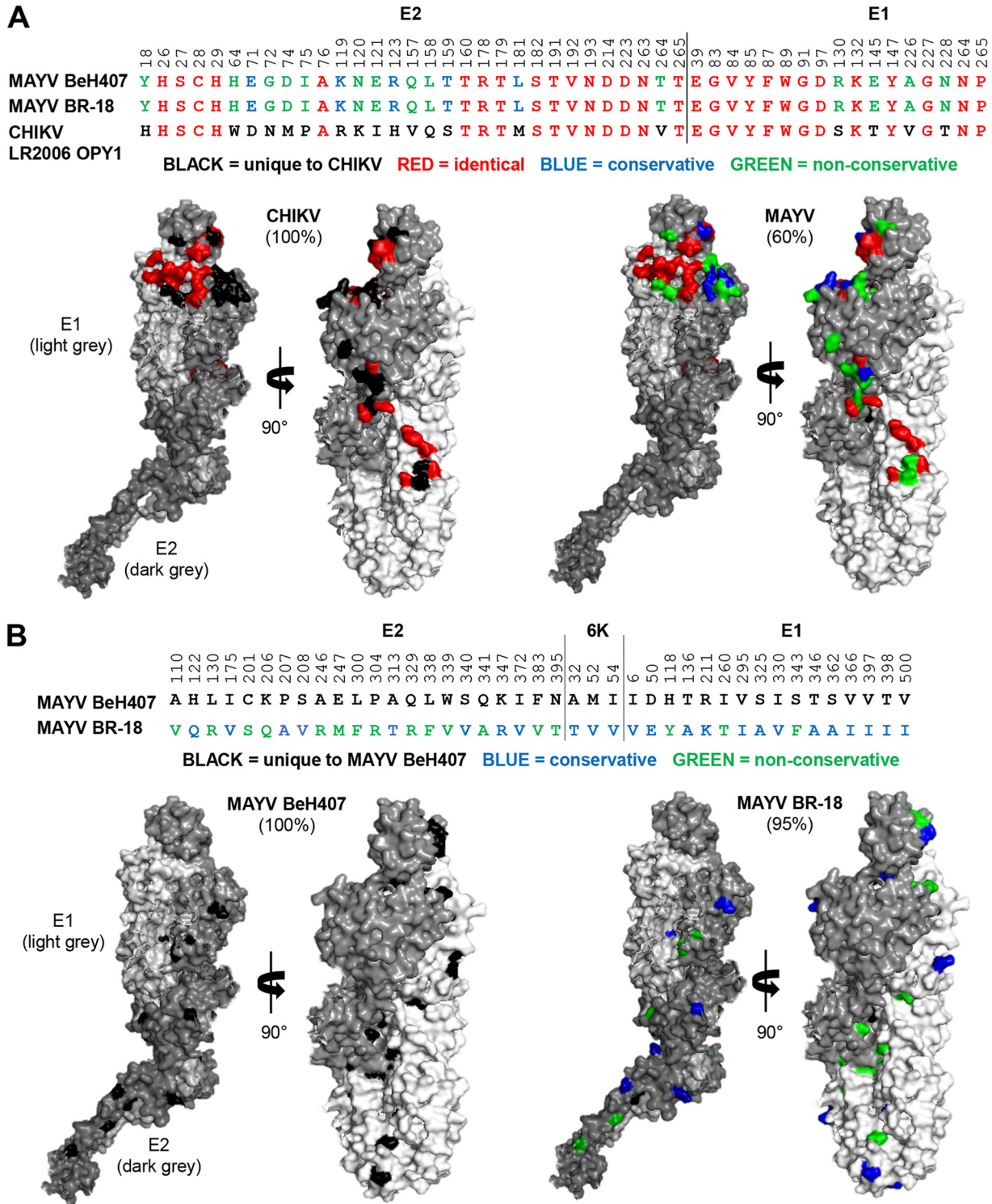


FIG 5 Sequencing of the contemporary isolate, BR-18. (A, top) The E1/E2 amino acids that make contact with the receptor MXRA8 are identical for the two MAYV isolates, showing 60% amino acid identity with CHIKV (Reunion Island isolate). (Bottom) The crystal structure of CHIKV E1/E2 dimer, with the receptor contact residues that differed between MAYV and CHIKV colored as above. (B, top) Differences between the two MAYV isolates in E1/E2 (these amino acids are believed not to be involved in interaction with the receptor). (Bottom) The crystal structure of CHIKV E1/E2 dimer, with the residues that differed between the two isolates colored as above.

Sequencing of the BR-18 isolate indicated that MAYV continues to evolve, although BR-18 did not contain the E2-T179N substitution recently suggested as an adaptation toward *Aedes aegypti* transmission (8). BR-18 segregated with genotype D isolates (Fig. S2), and taken together with the neutralization data, this argues a genotype L vaccine should cross-protect against genotype D viruses. A similar “single-serogroup contention” has been made for CHIKV, despite the existence of different genotypes and lineages (70, 71). Nevertheless, BR-18 shows significant divergence from other genotype D viruses, sitting between genotype D and L viruses, perhaps arguing that MAYV genotype classifications may need reevaluation as more sequences become available.

The baculovirus-insect cell expression system has already proven to be a suitable large-scale platform for the production of licensed human vaccines, including an influenza virus hemagglutinin subunit vaccine (Flublok, Sanofi) (72), a human papillomavirus VLP vaccine (Cervarix, GlaxoSmithKline) (73), and a registered vaccine against 2019 coronavirus disease (Nuvaxovid, Novavax) (74), demonstrating the utility of the platform. However, a MAYV vaccine would currently not be commercially viable due to the small market size (22), although this could rapidly change if MAYV follows in the footsteps of CHIKV and ZIKV to become a virus of international concern (23, 75).

MATERIALS AND METHODS

Ethics statement. All mouse work was conducted in accordance with the Australian code for the care and use of animals for scientific purposes as defined by the National Health and Medical Research Council of Australia. Mouse work was approved by the QIMR Berghofer Medical Research Institute animal ethics committee (P2235 A1606-618M).

Cell culture. The *Spodoptera frugiperda*-derived cell lines Sf21 (Gibco, Carlsbad, CA, USA), Sf9 (Gibco), and Sf9-ET (76) were grown at 27°C. Monolayers of Sf21 cells were grown in Grace's medium (Gibco) supplemented with 10% fetal bovine serum (FBS; Gibco). Monolayers of Sf9-ET cells were grown in Sf900II medium (Gibco) supplemented with 5% FBS and 100 µg/mL Geneticin (Gibco). Monolayers and suspension cultures of Sf9 cells were grown in Sf900II serum-free medium supplemented with 50 µg/mL gentamicin (Gibco). The *Aedes albopictus*-derived cell line C6/36 was cultured in RPMI 1640 medium (Thermo Fisher Scientific, Scoresby, VIC, Australia) with 10% FBS (Sigma-Aldrich, Castle Hill, NSW, Australia) at 28°C and 5% CO₂. The African green monkey kidney Vero cell line was maintained in RPMI 1640 medium supplemented with 10% FBS at 37°C and 5% CO₂.

Viruses. The 1955 MAYV isolate BeH407 (GenBank accession number [MK573238.1](#)) was a generous gift from M. S. Diamond (Washington University School of Medicine, St. Louis, MO, USA). The contemporary MAYV isolate BR-18 (Brazil 2018) was a generous gift from Renato Resende (University of Brasilia, Brazil; originally from Instituto Oswaldo Cruz, Rio de Janeiro, Brazil; strain Campos-RJ) (50). MAYV isolates and CHIKV strain Reunion (LR2006-OPY1; GenBank accession number [DQ443544](#)) were propagated on C6/36 cells and titrated by TCID₅₀ assays using C6/36 and Vero cell lines as described elsewhere (22, 68). Virus preparations were tested for endotoxin (77) and mycoplasma (MycoAlert, Lonza) (78).

Generation of recombinant baculovirus. Total RNA was isolated from MAYV BeH407-infected cells using TRIzol reagent (Invitrogen, Carlsbad, CA, USA). cDNA was generated using SuperScript II reverse transcriptase (Invitrogen). The complete structural cassette of MAYV (C-E3-E2-6K-E1; 3,729 bp; GenBank accession number [MK573238.1](#)) was then amplified and provided with BamHI and HindIII restriction sites by PCR using Phusion high-fidelity DNA polymerase (New England Biolabs, Ipswich, MA, USA) and a 2720 thermal cycler (Applied Biosystems, Foster City, CA, USA). Next, the Bac-to-Bac baculovirus-insect cell expression system (Invitrogen) was used to insert the structural cassette of MAYV into the improved *Autographa californica* multiple capsid nucleopolyhedrovirus backbone BACe56 (79). The MAYV structural cassette was first ligated into pFastBac Dual (Invitrogen) behind the polyhedrin promoter and then transposed into BACe56. Transfection of Sf21 cells with purified recombinant bacmid DNA using ExpreS² TR (ExpreS²ion Biotechnologies, Hørsholm, Denmark) resulted in the recovery of recombinant baculovirus. Virus titers (in TCID₅₀ per milliliter) were measured using Sf9-ET cells.

MAYV VLP production and purification. For small-scale MAYV VLP production, 8 × 10⁶ Sf9 cells were seeded as a monolayer in a 75-cm² flask. Cells were infected with recombinant baculovirus containing the MAYV structural cassette (BACe56/MAYV) at an MOI of 2 TCID₅₀ units per cell. After infection, cells were incubated for 4 h at 27°C, and medium was replaced by fresh Sf900II serum-free medium. For large-scale MAYV VLP production, 10 Sf9 suspension cultures of 50 mL each containing 2.6 × 10⁶ cells/mL were infected with BACe56/MAYV at an MOI of ≈0.2 TCID₅₀ units per cell. Cells were incubated at 27°C for 4 days, and cells and medium were then separated by centrifugation at 1,700 rpm for 5 min. The cell pellet was dissolved in phosphate-buffered saline (PBS). The supernatant containing the MAYV VLPs was first filtered through a filter with a pore size of 0.45 µm, and then 7% (wt/vol) PEG-6000 and 0.5 M NaCl were added to the filtered medium to precipitate the VLPs. After 2 h at room temperature (RT) and subsequent centrifugation at 4,700 rpm for 15 min, the pellet was dissolved in GTNE buffer (200 mM glycine, 50 mM Tris-HCl, 100 mM NaCl, 1 mM EDTA; pH 7.3). VLPs were then purified on a discontinuous sucrose gradient (40% to 70% [wt/vol]) as described previously (36, 41).

MAYV protein analysis. MAYV proteins from infected cell fractions and pure VLP fractions were detected using sodium dodecyl sulfate-polyacrylamide gel electrophoresis (SDS-PAGE) and subsequent western blotting. Loading buffer containing SDS and β -mercaptoethanol was added to the samples followed by incubations for 10 min at 95°C. After centrifugation for 1 min at 14,000 rpm, samples were run on a Mini-Protean TGX gel (Bio-Rad, Veenendaal, the Netherlands). Proteins were transferred to an Immobilon-P membrane (Merck Millipore, Darmstadt, Germany) using a trans-blot semidry transfer cell (Bio-Rad). The membrane was blocked at 4°C overnight using 1% skimmed milk powder in PBS containing 0.05% Tween (PBS-T). The membrane was incubated with either convalescent polyclonal antiserum from a MAYV-infected mouse, diluted 1:250 in 1% skimmed milk, or the anti-CHIKV capsid 5.5D11 monoclonal antibody (43), diluted 1:500 in 1% skimmed milk. After 1 h, the membrane was washed three times with PBS-T. The membrane was incubated with alkaline phosphatase-conjugated goat anti-mouse IgG secondary antibody (Sigma-Aldrich, Darmstadt, Germany) for 1 h. Secondary antibody was diluted 1:2,500 in PBS-T. After washing three times with PBS-T, the membrane was incubated with alkaline phosphatase buffer as described previously (36) for 10 min. The membrane was then developed using nitroblue tetrazolium-5-bromo-4-chloro-3-indolylphosphate (Roche Diagnostics, Almere, the Netherlands).

MAYV VLP quantification. The purified MAYV VLPs produced in Sf9 insect cells (named WUR MAYV VLPs) were quantified using a dilution series of pure MAYV VLPs from HEK293 human cells purchased at The Native Antigen Company (Oxford, UK). TNAC recombinant MAYV VLPs (strain Acre27) comprised E1 and E2, and capsid proteins (NCBI accession numbers [AJA37502.1](#) and [KM400591.1](#)) and were expressed in HEK293 cells. The VLPs included a mouse Fc tag and were buffered in Dulbecco's PBS at pH 7.4. Samples containing serial 2-fold dilutions of 0.5 μ g TNAC MAYV VLPs were prepared. These samples and the purified fraction containing WUR MAYV VLPs were analyzed using SDS-PAGE and western blotting with antiserum from a MAYV-infected mouse, as described above. Comparison of the band intensity for MAYV E2/E1 resulted in an estimated concentration of WUR MAYV VLPs in the purified fraction.

Transmission electron microscopy. Purified MAYV VLPs in GTNE buffer were loaded onto 200-mesh carbon-coated copper grids (Electron Microscopy Sciences, Hatfield, PA, USA). After 2 min at RT, the excess of liquid was removed and 2% ammonium molybdate (pH 6.8) was added to the grids for 30 s at RT. Next, the excess of liquid was removed and the grids were air dried. Grids were analyzed using a JEOL JEM-1400Plus transmission electron microscope. VLP diameters were measured using ImageJ (National Institutes of Health, Bethesda, MD, USA) in combination with in-house macros.

Mice, infection, virus titration, and disease evaluation. Mice were kept under the following conditions: 12:12 light-dark cycle; 7:45 a.m. sunrise and 7:45 pm sunset; 15-min light-dark dark-light ramping times. Enclosures were M.I.C.E cages (Animal Care Systems, Centennial, CO, USA). Ventilation was with 100% fresh air, 8 complete air exchanges/h/room. Temperature was $22 \pm 1^\circ\text{C}$. In-house enrichment used paper cups, tissue paper, and cardboard rolls. Bedding was PuraChips (Able Scientific, Perth, WA, Australia) (aspen fine). Food was double-bagged Norco rat and mouse pellet (AIRR, Darra, QLD, Australia). Water was deionized water acidified with HCl (pH = 3.2).

To establish the model, female C57BL/6J mice (6 to 24 weeks old) were purchased from the Animal Resources Centre (Canning Vale, WA, Australia). Mice were infected with 10^4 to 10^6 TCID₅₀ of MAYV BeH407 subcutaneously into the top or side of each hind foot as described previously (22, 48, 68). Serum viremia, foot swelling, and histology were evaluated as described previously (22, 48, 51, 68, 80).

MAYV VLP vaccination and virus challenge. The WUR MAYV VLP, derived from Sf9 insect cells, and the TNAC MAYV VLP, derived from HEK293 human cells, were used to vaccinate mice (female C57BL/6J, 6 to 8 weeks old). The adjuvant comprised QS-21 (50 μ g/mL; Creative Biolabs, Shirley, NY, USA), 3-*O*-desacyl-4'-monophosphoryl lipid A (MPLA; 50 μ g/mL), cholesterol (250 μ g/mL), and dioleoyl phosphatidylcholine (1 mg/mL; Sigma-Aldrich) constituted in PBS by sonication as described elsewhere (49). The WUR MAYV VLP was mixed with adjuvant (1:1 [vol/vol]) for a total dose of 1 μ g of VLP and 1 μ g of adjuvant per mouse. The vaccines (with or without adjuvant) were mixed with RPMI 1640 medium and administered intramuscularly as described elsewhere (22), with the dose split equally into both quadriceps muscles of restrained mice with 50 μ L per muscle using an insulin syringe (Becton, Dickinson, NJ, USA). Vaccinated mice were challenged with 10^5 TCID₅₀ of MAYV BeH407 into each hind foot, and viremia, foot swelling, and histology were evaluated as described above.

Antibody ELISA and neutralization assays. IgG responses were determined by standard ELISA using whole MAYV BeH407 as antigen. The antigen was purified from infected C6/36 cell supernatants by 40% PEG-6000 precipitation (Sigma-Aldrich) and ultracentrifugation (Beckman floor standing ultra, Beckman Coulter, CA, USA) at $\sim 134,000$ rcf at 4°C for 2 h through a 20% sucrose (Sigma-Aldrich) cushion. Endpoint ELISA titers were determined as described previously (22, 81, 82). Briefly, serum samples, starting at a 1:30 dilution, were serially diluted 1:3 in duplicate and bound antibody detected using biotin-labeled rat anti-mouse-IgG (Thermo Fisher Scientific), streptavidin HRP (Biosource, Camarillo, CA, USA), and 2,2'-azino-bis(3-ethylbenzothiazolonesulfonic acid) substrate (Sigma-Aldrich). Endpoint titers were interpolated when optical density at 450 nm (OD₄₅₀) values reached the mean OD₄₅₀ + 3 standard errors of the mean for naive serum. Neutralization assays were performed as described elsewhere (22, 81). Briefly, mouse serum samples were heat-inactivated (56°C for 30 min) and incubated in duplicate with 150 TCID₅₀ of MAYV BeH407, MAYV BR-18, or CHIKV at 37°C for 1 h before Vero cells were added at a concentration of 10^5 cells/well. The initial serum dilution was 1:10, with serial dilutions of 1:2 in duplicate. After 5 days, cells were fixed and stained with formaldehyde and crystal violet, and the 50% (and 80% [Fig. S4]) neutralizing titers were interpolated from optical density (OD₅₉₀) values versus serum dilution plots, as described elsewhere (22, 82).

Histology. Histology and quantitation of staining were undertaken as described previously (22, 48, 51, 68, 80). In brief, feet were fixed in 10% formalin, decalcified with EDTA (Sigma-Aldrich), and embedded in

paraffin (Sigma-Aldrich), and sections were stained with H&E (Sigma-Aldrich). Slides were scanned using Aperio AT Turbo (Aperio, Vista, CA, USA) and analyzed using Aperio ImageScope v10 software (Leica Biosystems, Waverley, Australia) and the Positive Pixel Count v9 algorithm.

Sequencing and structure visualizations. Trizol (Invitrogen) was added to BR-18-infected C6/36 cells, and RNA was purified as per the manufacturer's instructions. RNA sequencing (RNA-Seq) and subsequent analyses were undertaken essentially as described before (83). Briefly, RNA-Seq used an in-house Illumina Nextseq 550 platform to generate 75-bp paired-end reads. The per base sequence quality for >90% bases was above Q30. The quality of raw sequencing reads was assessed using FastQC (v0.11.80), and trimmed using Cutadapt (v2.3) to remove adapter sequences and low-quality bases. Trimmed reads were aligned using STAR (v2.7.1a) to a combined reference of *Aedes albopictus* (NW_021837045.1) and MAYV (AF237947.1) genomes. SAMtools mpileup was used to produce a consensus sequence from mapped viral reads (GenBank accession number OP628214).

Phylogenetic trees were constructed as described previously (82) using MEGA-X (Molecular Evolutionary Genetics Analysis 10, Penn State University, State College, PA, USA) and the ClustalW plugin with default parameters. Phylogenetic trees were constructed using the maximum-likelihood method, for nucleotide sequences with the General Time Reversible model and for amino acid sequences using the JTT matrix-based model. The trees were rooted using the CHIKV Reunion Island isolate. E1/E2 dimer structure visualizations were generated using PyMOL Molecular Graphics System (version 2.3.3; Schrodinger, NY, USA) using the structure of PDB 7K08 (84).

Statistics. Statistical analyses were performed using IBM SPSS Statistics for Windows v19.0 (IBM Corp., Armonk, NY, USA). The *t* test was used when the difference in variances was <4, skewness was >-2, and kurtosis was <2. Otherwise, the nonparametric Kolmogorov-Smirnov test was used.

Data availability. Raw viral RNA-seq data have been uploaded to NCBI SRA under BioProject accession number PRJNA935483.

SUPPLEMENTAL MATERIAL

Supplemental material is available online only.

SUPPLEMENTAL FILE 1, PDF file, 3 MB.

ACKNOWLEDGMENTS

We thank Jan van Lent, Marcel Giesbers, and Jelmer Vroom for their assistance with electron microscopy, Els Roode for cell culture maintenance, Victor van Gelder for his contribution to the design of the MAYV structural cassette construct, the QIMR Berghofer animal house for their assistance, Clay Winterford and Sang-Hee Park for their assistance with histology, Roy Hall and Jody Hobson-Peters for providing the antibody 5.5D11, Renato Resende for providing the MAYV BR-18 isolate, and Michael Diamond for providing RNA of the MAYV BeH407 isolate. Thanks to D. Rawle for assistance with student supervision.

We declare no financial conflicts of interest.

S.R.A. was supported by ZonMw (project ZikaRisk "Risk of Zika virus introductions for the Netherlands," grant number 522003001) and by the graduate school PE&RC via a strategic fund award. W.N. was awarded a Research Training Program PhD scholarship from the Faculty of Medicine, University of Queensland, Australia, and a QIMR Berghofer Top Up Scholarship from the Higher Degrees Committee at QIMR Berghofer. The work was also supported by a project grant from the National Health and Medical Research Council (NHMRC) of Australia (APP1078468) and intramural seed funding from the Australian Infectious Disease Research Centre. A.S. is supported by an Investigator Grant from the NHMRC (APP1173880). The funders had no role in study design, data collection and interpretation, or the decision to submit the work for publication.

Investigation: S.R.A., W.N., M.H.C.A.-H., D.V.D.K., N.H.A.S., C.G., T.T.T.L., B.T., and K.Y.; Formal Analysis: S.R.A., W.N., T.D., and A.S.; Funding Acquisition: S.R.A., M.M.V.O., A.S., and G.P.P.; Supervision: M.M.V.O., A.S., and G.P.P.; Writing – Original Draft: S.R.A. and W.N.; Writing – Review and Editing: S.R.A., W.N., M.M.V.O., A.S., and G.P.P.

REFERENCES

1. Suhrbier A. 2019. Rheumatic manifestations of chikungunya: emerging concepts and interventions. *Nat Rev Rheumatol* 15:597–611. <https://doi.org/10.1038/s41584-019-0276-9>.
2. Weaver SC, Forrester NL. 2015. Chikungunya: evolutionary history and recent epidemic spread. *Antiviral Res* 120:32–39. <https://doi.org/10.1016/j.antiviral.2015.04.016>.
3. Nakayama E, Kato F, Tajima S, Ogawa S, Yan K, Takahashi K, Sato Y, Suzuki T, Kawai Y, Inagaki T, Taniguchi S, Le TT, Tang B, Prow NA, Uda A, Maeki T, Lim CK, Khromykh AA, Suhrbier A, Saijo M. 2021. Neuroinvasiveness of the MR766 strain of Zika virus in IFNAR^{-/-} mice maps to prM residues conserved amongst African genotype viruses. *PLoS Pathog* 17:e1009788. <https://doi.org/10.1371/journal.ppat.1009788>.

4. Musso D, Gubler DJ. 2016. Zika virus. *Clin Microbiol Rev* 29:487–524. <https://doi.org/10.1128/CMR.00072-15>.
5. Celone M, Okech B, Han BA, Forshey BM, Anyamba A, Dunford J, Rutherford G, Mita-Mendoza NK, Estallo EL, Khouri R, de Siqueira IC, Pollett S. 2021. A systematic review and meta-analysis of the potential non-human animal reservoirs and arthropod vectors of the Mayaro virus. *PLoS Negl Trop Dis* 15:e0010016. <https://doi.org/10.1371/journal.pntd.0010016>.
6. Diagne CT, Bengue M, Choumet V, Hamel R, Pompon J, Misse D. 2020. Mayaro virus pathogenesis and transmission mechanisms. *Pathogens* 9: 738. <https://doi.org/10.3390/pathogens9090738>.
7. Hoch AL, Peterson NE, LeDuc JW, Pinheiro FP. 1981. An outbreak of Mayaro virus disease in Belterra, Brazil. III. Entomological and ecological studies. *Am J Trop Med Hyg* 30:689–698. <https://doi.org/10.4269/ajtmh.1981.30.689>.
8. Roesch F, Cereghino C, Carrau L, Hardy A, Ribeiro-Filho H, Lacritick AH, Koh C, Marano J, Bates T, Rai P, Chuong C, Akter S, Vallet T, Blanc H, Elliot T, Brown AM, Michalak P, LeRoith T, Bloom J, Marques RE, Saleh M-C, Vignuzzi M, Weger-Lucarelli J. 2022. The E2 glycoprotein holds key residues for Mayaro virus adaptation to the urban *Aedes aegypti* mosquito. <https://www.biorxiv.org/content/10.1101/2022.04.05.487100v1>.
9. de Curcio JS, Salem-Izacc SM, Pereira Neto LM, Nunes EB, Anunciacao CE, Silveira-Lacerda EP. 2022. Detection of Mayaro virus in *Aedes aegypti* mosquitoes circulating in Goiania-Goiias-Brazil. *Microbes Infect* 24:104948. <https://doi.org/10.1016/j.micinf.2022.104948>.
10. Alomar AA, Alto BW. 2022. Temperature-mediated effects on Mayaro virus vector competency of Florida *Aedes aegypti* mosquito vectors. *Viruses* 14: 880. <https://doi.org/10.3390/v14050880>.
11. Dieme C, Ciota AT, Kramer LD. 2020. Transmission potential of Mayaro virus by *Aedes albopictus*, and *Anopheles quadrimaculatus* from the USA. *Parasit Vectors* 13:613. <https://doi.org/10.1186/s13071-020-04478-4>.
12. Long KC, Ziegler SA, Thangamani S, Hausser NL, Kochel TJ, Higgs S, Tesh RB. 2011. Experimental transmission of Mayaro virus by *Aedes aegypti*. *Am J Trop Med Hyg* 85:750–757. <https://doi.org/10.4269/ajtmh.2011.11-0359>.
13. Wiggans K, Eastmond B, Alto BW. 2018. Transmission potential of Mayaro virus in Florida *Aedes aegypti* and *Aedes albopictus* mosquitoes. *Med Vet Entomol* 32:436–442. <https://doi.org/10.1111/mve.12322>.
14. Pereira TN, Carvalho FD, De Mendonca SF, Rocha MN, Moreira LA. 2020. Vector competence of *Aedes aegypti*, *Aedes albopictus*, and *Culex quinquefasciatus* mosquitoes for Mayaro virus. *PLoS Negl Trop Dis* 14:e0007518. <https://doi.org/10.1371/journal.pntd.0007518>.
15. Mutricy R, Matheus S, Mosnier E, Martinez-Lorenzi E, De Laval F, Nacher M, Niemetzky F, Naudion P, Djossou F, Rousset D, Epelboin L. 2022. Mayaro virus infection in French Guiana, a cross sectional study 2003–2019. *Infect Genet Evol* 99:105243. <https://doi.org/10.1016/j.meegid.2022.105243>.
16. Julia da Silva Pessoa Vieira C, Jose Ferreira da Silva D, Rigotti Kubiszkeski J, Ceschini Machado L, Pena LJ, Vieira de Moraes Bronzoni R, da Luz Wallau G. 2020. The emergence of chikungunya ECSA lineage in a Mayaro endemic region on the southern border of the Amazon Forest. *TropicalMed* 5:105. <https://doi.org/10.3390/tropicalmed5020105>.
17. Llagonne-Barets M, Icard V, Leparac-Goffart I, Prat C, Perpoint T, Andre P, Ramiere C. 2016. A case of Mayaro virus infection imported from French Guiana. *J Clin Virol* 77:66–68. <https://doi.org/10.1016/j.jcv.2016.02.013>.
18. Tesh RB, Watts DM, Russell KL, Damodaran C, Calampa C, Cabezas C, Ramirez G, Vasquez B, Hayes CG, Rossi CA, Powers AM, Hice CL, Chandler LJ, Cropp BC, Karabatsos N, Roehrig JT, Gubler DJ. 1999. Mayaro virus disease: an emerging mosquito-borne zoonosis in tropical South America. *Clin Infect Dis* 28:67–73. <https://doi.org/10.1086/515070>.
19. Lednicky J, De Rochars VM, Elbadry M, Loeb J, Telisma T, Chavannes S, Anilis G, Cella E, Cicozzi M, Okech B, Salemi M, Morris JG, Jr. 2016. Mayaro virus in child with acute febrile illness, Haiti, 2015. *Emerg Infect Dis* 22: 2000–2002. <https://doi.org/10.3201/eid2211.161015>.
20. Suhrbier A, Jaffar-Bandjee MC, Gasque P. 2012. Arthritogenic alphaviruses: an overview. *Nat Rev Rheumatol* 8:420–429. <https://doi.org/10.1038/nrrheum.2012.64>.
21. Zaid A, Burt FJ, Liu X, Poo YS, Zandi K, Suhrbier A, Weaver SC, Texeira MM, Mahalingam S. 2021. Arthritogenic alphaviruses: epidemiological and clinical perspective on emerging arboviruses. *Lancet Infect Dis* 21:e123–e133. [https://doi.org/10.1016/S1473-3099\(20\)30491-6](https://doi.org/10.1016/S1473-3099(20)30491-6).
22. Nguyen W, Nakayama E, Yan K, Tang B, Le TT, Liu L, Cooper TH, Hayball JD, Faddy HM, Warrilow D, Allcock RJN, Hobson-Peters J, Hall RA, Rawle DJ, Lutzy VP, Young P, Oliveira NM, Hartel G, Howley PM, Prow NA, Suhrbier A. 2020. Arthritogenic alphavirus vaccines: serogrouping versus cross-protection in mouse models. *Vaccines* 8:209. <https://doi.org/10.3390/vaccines8020209>.
23. Acosta-Ampudia Y, Monsalve DM, Rodriguez Y, Pacheco Y, Anaya JM, Ramirez-Santana C. 2018. Mayaro: an emerging viral threat? *Emerg Microbes Infect* 7:1–11. <https://doi.org/10.1038/s41426-018-0163-5>.
24. Strauss JH, Strauss EG. 1994. The alphaviruses: gene expression, replication, and evolution. *Microbiol Rev* 58:491–562. <https://doi.org/10.1128/mr.58.3.491-562.1994>.
25. Firth AE, Chung BY, Fleeton MN, Atkins JF. 2008. Discovery of frameshifting in alphavirus 6K resolves a 20-year enigma. *Virology* 375:108. <https://doi.org/10.1186/1743-422X-5-108>.
26. Jose J, Snyder JE, Kuhn RJ. 2009. A structural and functional perspective of alphavirus replication and assembly. *Future Microbiol* 4:837–856. <https://doi.org/10.2217/fmb.09.59>.
27. Li L, Jose J, Xiang Y, Kuhn RJ, Rossmann MG. 2010. Structural changes of envelope proteins during alphavirus fusion. *Nature* 468:705–708. <https://doi.org/10.1038/nature09546>.
28. Weise WJ, Hermance ME, Forrester N, Adams AP, Langsjoen R, Gorchakov R, Wang E, Alcorn MD, Tsetsarkin K, Weaver SC. 2014. A novel live-attenuated vaccine candidate for Mayaro fever. *PLoS Negl Trop Dis* 8:e2969. <https://doi.org/10.1371/journal.pntd.0002969>.
29. Mota MTO, Costa VV, Sugimoto MA, Guimaraes GF, Queiroz-Junior CM, Moreira TP, de Sousa CD, Santos FM, Queiroz VF, Passos I, Hubner J, Souza DG, Weaver SC, Teixeira MM, Nogueira ML. 2020. In-depth characterization of a novel live-attenuated Mayaro virus vaccine candidate using an immunocompetent mouse model of Mayaro disease. *Sci Rep* 10:5306. <https://doi.org/10.1038/s41598-020-62084-x>.
30. Choi H, Kudchodkar SB, Reuschel EL, Asija K, Borole P, Ho M, Wojtak K, Reed C, Ramos S, Bopp NE, Aguilar PV, Weaver SC, Kim JJ, Humeau L, Tebas P, Weiner DB, Muthumani K. 2019. Protective immunity by an engineered DNA vaccine for Mayaro virus. *PLoS Negl Trop Dis* 13:e0007042. <https://doi.org/10.1371/journal.pntd.0007042>.
31. Campos RK, Preciado-Llanes L, Azar SR, Kim YC, Brandon O, Lopez-Camacho C, Reyes-Sandoval A, Rossi SL. 2020. Adenoviral-vectored Mayaro and chikungunya virus vaccine candidates afford partial cross-protection from lethal challenge in A129 mouse model. *Front Immunol* 11:591885. <https://doi.org/10.3389/fimmu.2020.591885>.
32. Powers JM, Haese NN, Denton M, Ando T, Krecklywich C, Bonin K, Streblov CE, Krecklywich N, Smith P, Broeckel R, DeFilippis V, Morrison TE, Heise MT, Streblov DN. 2021. Non-replicating adenovirus based Mayaro virus vaccine elicits protective immune responses and cross protects against other alphaviruses. *PLoS Negl Trop Dis* 15:e0009308. <https://doi.org/10.1371/journal.pntd.0009308>.
33. Edelman R, Tacket CO, Wasserman SS, Bodison SA, Perry JG, Mangiafico JA. 2000. Phase II safety and immunogenicity study of live chikungunya virus vaccine TSI-GSD-218. *Am J Trop Med Hyg* 62:681–685. <https://doi.org/10.4269/ajtmh.2000.62.681>.
34. Hobernik D, Bros M. 2018. DNA vaccines: how far from clinical use? *Int J Mol Sci* 19:3605. <https://doi.org/10.3390/ijms19113605>.
35. Chang J. 2021. Adenovirus vectors: excellent tools for vaccine development. *Immune Netw* 21:e6. <https://doi.org/10.4110/in.2021.21.e6>.
36. Metz SW, Gardner J, Geertsema C, Le TT, Goh L, Vlak JM, Suhrbier A, Pijlman GP. 2013. Effective chikungunya virus-like particle vaccine produced in insect cells. *PLoS Negl Trop Dis* 7:e2124. <https://doi.org/10.1371/journal.pntd.0002124>.
37. Grgacic EV, Anderson DA. 2006. Virus-like particles: passport to immune recognition. *Methods* 40:60–65. <https://doi.org/10.1016/j.ymeth.2006.07.018>.
38. Pijlman GP. 2015. Enveloped virus-like particles as vaccines against pathogenic arboviruses. *Biotechnol J* 10:659–670. <https://doi.org/10.1002/biot.201400427>.
39. Xiang SD, Scholzen A, Minigo G, David C, Apostolopoulos V, Mottram PL, Plebanski M. 2006. Pathogen recognition and development of particulate vaccines: does size matter? *Methods* 40:1–9. <https://doi.org/10.1016/j.ymeth.2006.05.016>.
40. Mohsen MO, Bachmann MF. 2022. Virus-like particle vaccinology, from bench to bedside. *Cell Mol Immunol* 19:993–1011. <https://doi.org/10.1038/s41423-022-00897-8>.
41. Metz SW, Pijlman GP. 2016. Production of chikungunya virus-like particles and subunit vaccines in insect cells. *Methods Mol Biol* 1426:297–309. https://doi.org/10.1007/978-1-4939-3618-2_27.
42. Hikke MC, Geertsema C, Wu V, Metz SW, van Lent JW, Vlak JM, Pijlman GP. 2016. Alphavirus capsid proteins self-assemble into core-like particles in

- insect cells: a promising platform for nanoparticle vaccine development. *Biotechnol J* 11:266–273. <https://doi.org/10.1002/biot.201500147>.
43. Goh LYH, Hobson-Peters J, Prow NA, Gardner J, Bielefeldt-Ohmann H, Suhrbier A, Hall RA. 2015. Monoclonal antibodies specific for the capsid protein of chikungunya virus suitable for multiple applications. *J Gen Virol* 96:507–512. <https://doi.org/10.1099/jgv.0.000002>.
 44. Wagner JM, Pajerowski JD, Daniels CL, McHugh PM, Flynn JA, Balliet JW, Casimiro DR, Subramanian S. 2014. Enhanced production of chikungunya virus-like particles using a high-pH adapted *Spodoptera frugiperda* insect cell line. *PLoS One* 9:e94401. <https://doi.org/10.1371/journal.pone.0094401>.
 45. La Linn M, Gardner J, Warrilow D, Darnell GA, McMahon CR, Field I, Hyatt AD, Slade RW, Suhrbier A. 2001. Arbovirus of marine mammals: a new alphavirus isolated from the elephant seal louse, *Lepidophthirus macrorhini*. *J Virol* 75:4103–4109. <https://doi.org/10.1128/JVI.75.9.4103-4109.2001>.
 46. de Castro-Jorge LA, de Carvalho RVH, Klein TM, Hiroki CH, Lopes AH, Guimaraes RM, Fumagalli MJ, Floriano VG, Agostinho MR, Silhessarenko RD, Ramalho FS, Cunha TM, Cunha FQ, da Fonseca BAL, Zamboni DS. 2019. The NLRP3 inflammasome is involved with the pathogenesis of Mayaro virus. *PLoS Pathog* 15:e1007934. <https://doi.org/10.1371/journal.ppat.1007934>.
 47. Rulli NE, Guglielmotti A, Mangano G, Rolph MS, Apicella C, Zaid A, Suhrbier A, Mahalingam S. 2009. Amelioration of alphavirus-induced arthritis and myositis in a mouse model by treatment with bindarit, an inhibitor of monocyte chemotactic proteins. *Arthritis Rheum* 60:2513–2523. <https://doi.org/10.1002/art.24682>.
 48. Poo YS, Rudd PA, Gardner J, Wilson JA, Larcher T, Colle MA, Le TT, Nakaya HI, Warrilow D, Allcock R, Bielefeldt-Ohmann H, Schroder WA, Khromykh AA, Lopez JA, Suhrbier A. 2014. Multiple immune factors are involved in controlling acute and chronic chikungunya virus infection. *PLoS Negl Trop Dis* 8:e3354. <https://doi.org/10.1371/journal.pntd.0003354>.
 49. Yan K, Vet LJ, Tang B, Hobson-Peters J, Rawle DJ, Le TT, Larcher T, Hall RA, Suhrbier A. 2020. A yellow fever virus 17D infection and disease mouse model used to evaluate a chimeric Binjari-yellow fever virus vaccine. *Vaccines* 8:368. <https://doi.org/10.3390/vaccines8030368>.
 50. Vasconcellos AF, Mandacaru SC, de Oliveira AS, Fontes W, Melo RM, de Sousa MV, Resende RO, Charneau S. 2020. Dynamic proteomic analysis of *Aedes aegypti* Aag-2 cells infected with Mayaro virus. *Parasit Vectors* 13:297. <https://doi.org/10.1186/s13071-020-04167-2>.
 51. Rudd PA, Wilson J, Gardner J, Larcher T, Babarit C, Le TT, Anraku I, Kumagai Y, Loo YM, Gale M, Jr, Akira S, Khromykh AA, Suhrbier A. 2012. Interferon response factors 3 and 7 protect against chikungunya virus hemorrhagic fever and shock. *J Virol* 86:9888–9898. <https://doi.org/10.1128/JVI.00956-12>.
 52. Basore K, Kim AS, Nelson CA, Zhang R, Smith BK, Uranga C, Vang L, Cheng M, Gross ML, Smith J, Diamond MS, Fremont DH. 2019. Cryo-EM structure of chikungunya virus in complex with the Mxra8 receptor. *Cell* 177:1725–1737.e16. <https://doi.org/10.1016/j.cell.2019.04.006>.
 53. Miyata T, Miyazawa S, Yasunaga T. 1979. Two types of amino acid substitutions in protein evolution. *J Mol Evol* 12:219–236. <https://doi.org/10.1007/BF01732340>.
 54. Auguste AJ, Liria J, Forrester NL, Giambalvo D, Moncada M, Long KC, Moron D, de Manzione N, Tesh RB, Halsey ES, Kochel TJ, Hernandez R, Navarro JC, Weaver SC. 2015. Evolutionary and ecological characterization of Mayaro virus strains isolated during an outbreak, Venezuela, 2010. *Emerg Infect Dis* 21:1742–1750. <https://doi.org/10.3201/eid2110.141660>.
 55. Martins KA, Gregory MK, Valdez SM, Sprague TR, Encinales L, Pacheco N, Cure C, Porras-Ramirez A, Rico-Mendoza A, Chang A, Pitt ML, Nasar F. 2019. Neutralizing antibodies from convalescent chikungunya virus patients can cross-neutralize Mayaro and Una viruses. *Am J Trop Med Hyg* 100:1541–1544. <https://doi.org/10.4269/ajtmh.18-0756>.
 56. Webb EM, Azar SR, Haller SL, Langsojen RM, Cuthbert CE, Ramjag AT, Luo H, Plante K, Wang T, Simmons G, Carrington CVF, Weaver SC, Rossi SL, Auguste AJ. 2019. Effects of chikungunya virus immunity on Mayaro virus disease and epidemic potential. *Sci Rep* 9:20399. <https://doi.org/10.1038/s41598-019-56551-3>.
 57. Ramsauer K, Schwameis M, Firbas C, Mullner M, Putnak RJ, Thomas SJ, Despres P, Tauber E, Jilma B, Tangy F. 2015. Immunogenicity, safety, and tolerability of a recombinant measles-virus-based chikungunya vaccine: a randomised, double-blind, placebo-controlled, active-comparator, first-in-man trial. *Lancet Infect Dis* 15:519–527. [https://doi.org/10.1016/S1473-3099\(15\)70043-5](https://doi.org/10.1016/S1473-3099(15)70043-5).
 58. Chen GL, Coates EE, Plummer SH, Carter CA, Berkowitz N, Conan-Cibotti M, Cox JH, Beck A, O'Callahan M, Andrews C, Gordon IJ, Larkin B, Lampley R, Kaltovich F, Gall J, Carlton K, Mendy J, Haney D, May J, Bray A, Bailer RT, Dowd KA, Brockett B, Gordon D, Koup RA, Schwartz R, Mascola JR, Graham BS, Pierson TC, Donastorg Y, Rosario N, Pape JW, Hoen B, Cabie A, Diaz C, Ledgerwood JE, VRC 704 Study Team. 2020. Effect of a chikungunya virus-like particle vaccine on safety and tolerability outcomes: a randomized clinical trial. *JAMA* 323:1369–1377. <https://doi.org/10.1001/jama.2020.2477>.
 59. Wressnigg N, Hochreiter R, Zoihs O, Fritzer A, Bézay N, Klingler A, Lingnau K, Schneider M, Lundberg U, Meinke A, Larcher-Senn J, Corbic-Ramljak I, Eder-Lingelbach S, Dubischar K, Bender W. 2020. Single-shot live-attenuated chikungunya vaccine in healthy adults: a phase 1, randomised controlled trial. *Lancet Infect Dis* 20:1193–1203. [https://doi.org/10.1016/S1473-3099\(20\)30238-3](https://doi.org/10.1016/S1473-3099(20)30238-3).
 60. Gavrillov BK, Rogers K, Fernandez-Sainz IJ, Holinka LG, Borca MV, Risatti GR. 2011. Effects of glycosylation on antigenicity and immunogenicity of classical swine fever virus envelope proteins. *Virology* 420:135–145. <https://doi.org/10.1016/j.virol.2011.08.025>.
 61. Fournillier A, Wychowski C, Boucreux D, Baumert TF, Meunier JC, Jacobs D, Muguet S, Depla E, Inchauspe G. 2001. Induction of hepatitis C virus E1 envelope protein-specific immune response can be enhanced by mutation of N-glycosylation sites. *J Virol* 75:12088–12097. <https://doi.org/10.1128/JVI.75.24.12088-12097.2001>.
 62. Kim HS, Jeon JH, Lee KJ, Ko K. 2014. N-glycosylation modification of plant-derived virus-like particles: an application in vaccines. *Biomed Res Int* 2014:249519. <https://doi.org/10.1155/2014/249519>.
 63. Lancaster C, Pristatsky P, Hoang VM, Casimiro DR, Schwartz RM, Rustandi R, Ha S. 2016. Characterization of N-glycosylation profiles from mammalian and insect cell derived chikungunya VLP. *J Chromatogr B Analyt Technol Biomed Life Sci* 1032:218–223. <https://doi.org/10.1016/j.jchromb.2016.04.025>.
 64. Hick TAH, Geertsema C, Henquet MGL, Martens DE, Metz SW, Pijlman GP. 2022. Secreted trimeric chikungunya virus spikes from insect cells: production, purification, and glycosylation status. *Processes* 10:162. <https://doi.org/10.3390/pr10010162>.
 65. Marek M, van Oers MM, Devaraj FF, Vlak JM, Merten OW. 2011. Engineering of baculovirus vectors for the manufacture of virion-free biopharmaceuticals. *Biotechnol Bioeng* 108:1056–1067. <https://doi.org/10.1002/bit.23028>.
 66. Prow NA, Liu L, Nakayama E, Cooper TH, Yan K, Eldi P, Hazlewood JE, Tang B, Le TT, Setoh YX, Khromykh AA, Hobson-Peters J, Diener KR, Howley PM, Hayball JD, Suhrbier A. 2018. A vaccinia-based single vector construct multi-pathogen vaccine protects against both Zika and chikungunya viruses. *Nat Commun* 9:1230. <https://doi.org/10.1038/s41467-018-03662-6>.
 67. Rawle DJ, Le TT, Dumenil T, Bishop C, Yan K, Nakayama E, Bird PI, Suhrbier A. 2022. Widespread discrepancy in Nnt genotypes and genetic backgrounds complicates granzyme A and other knockout mouse studies. *Elife* 11:e70207. <https://doi.org/10.7554/eLife.70207>.
 68. Gardner J, Anraku I, Le TT, Larcher T, Major L, Roques P, Schroder WA, Higgs S, Suhrbier A. 2010. Chikungunya virus arthritis in adult wild-type mice. *J Virol* 84:8021–8032. <https://doi.org/10.1128/JVI.02603-09>.
 69. Teo TH, Her Z, Tan JJ, Lum FM, Lee WW, Chan YH, Ong RY, Kam YW, Leparç-Goffart I, Gallian P, Renia L, de Lamballerie X, Ng LF. 2015. Caribbean and La Reunion chikungunya virus isolates differ in their capacity to induce proinflammatory Th1 and NK cell responses and acute joint pathology. *J Virol* 89:7955–7969. <https://doi.org/10.1128/JVI.00909-15>.
 70. Goo L, Dowd KA, Lin TY, Mascola JR, Graham BS, Ledgerwood JE, Pierson TC. 2016. A virus-like particle vaccine elicits broad neutralizing antibody responses in humans to all chikungunya virus genotypes. *J Infect Dis* 214:1487–1491. <https://doi.org/10.1093/infdis/jiw431>.
 71. Prow NA, Liu L, McCarthy MK, Walters K, Kalker R, Geiger J, Koide F, Cooper TH, Eldi P, Nakayama E, Diener KR, Howley PM, Hayball JD, Morrison TE, Suhrbier A. 2020. The vaccinia virus based Sementis Copenhagen vector vaccine against Zika and chikungunya is immunogenic in non-human primates. *NPJ Vaccines* 5:44. <https://doi.org/10.1038/s41541-020-0191-8>.
 72. Cox MM, Izikson R, Post P, Dunkle L. 2015. Safety, efficacy, and immunogenicity of Flublok in the prevention of seasonal influenza in adults. *Ther Adv Vaccines* 3:97–108. <https://doi.org/10.1177/2051013615595595>.
 73. Herrero R, Gonzalez P, Markowitz LE. 2015. Present status of human papillomavirus vaccine development and implementation. *Lancet Oncol* 16:e206–16. [https://doi.org/10.1016/S1470-2045\(14\)70481-4](https://doi.org/10.1016/S1470-2045(14)70481-4).
 74. Heath PT, Galiza EP, Baxter DN, Boffito M, Browne D, Burns F, Chadwick DR, Clark R, Cosgrove C, Galloway J, Goodman AL, Heer A, Higham A, Iyengar S, Jamal A, Jeanes C, Kalra PA, Kyriakidou C, McAuley DF, Meyrick A, Minassian AM, Minton J, Moore P, Munsoor I, Nicholls H, Osanlou O,

- Packham J, Pretswell CH, San Francisco Ramos A, Saralaya D, Sheridan RP, Smith R, Soiza RL, Swift PA, Thomson EC, Turner J, Viljoen ME, Albert G, Cho I, Dubovsky F, Glenn G, Rivers J, Robertson A, Smith K, Toback S, 2019nCoV-302 Study Group. 2021. Safety and efficacy of NVX-CoV2373 Covid-19 vaccine. *N Engl J Med* 385:1172–1183. <https://doi.org/10.1056/NEJMoa2107659>.
75. Aguilar-Luis MA, Del Valle-Mendoza J, Silva-Caso W, Gil-Ramirez T, Levy-Blitchein S, Bazan-Mayra J, Zavaleta-Gavidia V, Cornejo-Pacherras D, Palomares-Reyes C, Del Valle LJ. 2020. An emerging public health threat: Mayaro virus increases its distribution in Peru. *Int J Infect Dis* 92:253–258. <https://doi.org/10.1016/j.ijid.2020.01.024>.
76. Hopkins R, Esposito D. 2009. A rapid method for titrating baculovirus stocks using the Sf-9 Easy Titer cell line. *Biotechniques* 47:785–788. <https://doi.org/10.2144/000113238>.
77. Johnson BJ, Le TTT, Dobbin CA, Banovic T, Howard CB, Flores FdML, Vanags D, Naylor DJ, Hill GR, Suhrbier A. 2005. Heat shock protein 10 inhibits lipopolysaccharide-induced inflammatory mediator production. *J Biol Chem* 280:4037–4047. <https://doi.org/10.1074/jbc.M411569200>.
78. La Linn M, Bellett AJ, Parsons PG, Suhrbier A. 1995. Complete removal of mycoplasma from viral preparations using solvent extraction. *J Virol Methods* 52:51–54. [https://doi.org/10.1016/0166-0934\(94\)00136-5](https://doi.org/10.1016/0166-0934(94)00136-5).
79. Pijlman GP, Grose C, Hick TAH, Breukink HE, van den Braak R, Abbo SR, Geertsema C, van Oers MM, Martens DE, Esposito D. 2020. Relocation of the attTn7 transgene insertion site in bacmid DNA enhances baculovirus genome stability and recombinant protein expression in insect cells. *Viruses* 12:1448. <https://doi.org/10.3390/v12121448>.
80. Wilson JA, Prow NA, Schroder WA, Ellis JJ, Cumming HE, Gearing LJ, Poo YS, Taylor A, Hertzog PJ, Di Giallonardo F, Hueston L, Le Grand R, Tang B, Le TT, Gardner J, Mahalingam S, Roques P, Bird PI, Suhrbier A. 2017. RNA-Seq analysis of chikungunya virus infection and identification of granzyme A as a major promoter of arthritic inflammation. *PLoS Pathog* 13: e1006155. <https://doi.org/10.1371/journal.ppat.1006155>.
81. Wang D, Suhrbier A, Penn-Nicholson A, Woraratanadharm J, Gardner J, Luo M, Le TT, Anraku I, Sakalian M, Einfeld D, Dong JY. 2011. A complex adenovirus vaccine against chikungunya virus provides complete protection against viraemia and arthritis. *Vaccine* 29:2803–2809. <https://doi.org/10.1016/j.vaccine.2011.01.108>.
82. Rawle DJ, Nguyen W, Dumenil T, Parry R, Warrilow D, Tang B, Le TT, Slonchak A, Khromykh AA, Lutzky VP, Yan K, Suhrbier A. 2020. Sequencing of historical isolates, k-mer mining and high serological cross-reactivity with Ross River virus argue against the presence of Getah virus in Australia. *Pathogens* 9:848. <https://doi.org/10.3390/pathogens9100848>.
83. Rawle DJ, Le TT, Dumenil T, Yan K, Tang B, Nguyen W, Watterson D, Modhiran N, Hobson-Peters J, Bishop C, Suhrbier A. 2021. ACE2-lentiviral transduction enables mouse SARS-CoV-2 infection and mapping of receptor interactions. *PLoS Pathog* 17:e1009723. <https://doi.org/10.1371/journal.ppat.1009723>.
84. Song H, Zhao Z, Chai Y, Jin X, Li C, Yuan F, Liu S, Gao Z, Wang H, Song J, Vazquez L, Zhang Y, Tan S, Morel CM, Yan J, Shi Y, Qi J, Gao F, Gao GF. 2019. Molecular basis of arthritogenic alphavirus receptor MXRA8 binding to chikungunya virus envelope protein. *Cell* 177:1714–1724.e12. <https://doi.org/10.1016/j.cell.2019.04.008>.